Chalmers Publication Library

This document is the accepted manuscript version of a published work that appeared in final form in *Physical Chemistry Chemical Physics*, © Royal Society of Chemistry, after peer review and technical editing by the publisher. To access the final edited and published work, see http://dx.doi.org/10.1039/c000625d

(Article begins on next page)

Photophysical and structural properties of the fluorescent nucleobase analogues of the tricyclic cytosine (tC) family

Søren Preus,*[a] Kristine Kilså,[a] L. Marcus Wilhelmsson,[b] and Bo Albinsson*[b]

Received (in XXX, XXX) Xth XXXXXXXXX 200X, Accepted Xth XXXXXXXXX 200X
First published on the web Xth XXXXXXXXX 200X
DOI: 10.1039/b000000x

Fundamental insight into the unique fluorescence and nucleobase-mimicking properties of the fluorescent nucleobase analogues of the tC family is not only vital in explaining the behaviour of these probes in nucleic acid environments, but will also be profitable in the development of new and improved fluorescent base analogues. Here, temperature-dependent fluorescence quantum yield measurements are used to successfully separate and quantify the temperature-dependent and temperature–independent non-radiative excited-state decay processes of the three nucleobase analogues tC, tC^O and tC_{nitro}; all of which are derivatives of a phenothiazine or phenoxazine tricyclic framework. These results strongly suggest that the non-radiative decay process dominating the fast deactivation of tC_{nitro} is an internal conversion of a different origin than the decay pathways of tC and tC^O. tC_{nitro} is reported to be fluorescent only in less dipolar solvents at room temperature, which is explained by an increase in excited-state dipole moment along the main non-radiative decay pathway, a suggestion that apply in the photophysical discussion of large polycyclic nitroaromatics in general. New insight into the ground and excited-state potential energy surfaces of the isolated tC bases is obtained by means of high level DFT and TDDFT calculations. The S_0 potential energy surfaces of tC and tC_{nitro} possess two global minima corresponding to geometries folded along the middle sulphur–nitrogen axis separated by an energy barrier of 0.05 eV as calculated at the B3LYP/6-311+G(2d,p) level. The ground-state potential energy surface of tC^O is also predicted to be shallow along the bending coordinate but with an equilibrium geometry corresponding to the planar conformation of the tricyclic framework, which may explain some of the dissimilar properties of tC and tC^O in various confined (biological) environments. The S_1 equilibrium geometries of all three base analogues are predicted to be planar. These results are discussed in the context of the tC bases positioned in double-stranded DNA scenarios.

Notes and references

[a] *Department of Chemistry, University of Copenhagen, DK-2100 Copenhagen, Denmark; *E-mail: spreus@nano.ku.dk*
[b] *Department of Chemical and Biological Engineering/Physical Chemistry, Chalmers University of Technology, S-41296 Gothenburg, Sweden. *Fax: +46317723858; Tel: +46317723044; E-mail: balb@chalmers.se*

Introduction

The selection of synthetic fluorescent nucleobase analogues has grown considerably in recent years[1-4] with applications in areas ranging from quencher-free molecular beacons[5] and single-nucleotide polymorphism typing[5-7] to monitoring nucleic acid dynamics[8-14] and DNA-protein activity[15-26]. The ability to incorporate the fluorophore into nucleic acids as a replacement for one of the canonical bases offers a great advantage in the ability to position the reporter at a well-defined position close to or in the very site of interest. However, for by far the most fluorophores the base-stacking environment provided by double-stranded DNA introduces efficient non-radiative deactivation processes from the electronically excited states, such as charge transfer to neighbouring bases[27-28] and base collisions[29], often combined with a weaker oscillator strength of the lowest energy electronic transition[28, 30]. As a result, most fluorescent base analogues are highly or partly quenched in double-stranded DNA, a property accompanied by complex intensity decays greatly varying with neighbouring bases.[31-42] Whereas these features are useful for reporting on the local microenvironment of DNA, the low and variable fluorescence quantum yields are unsuitable features for fluorescence anisotropy and fluorescence resonance energy transfer (FRET) studies.[43] Equally important, these properties limit the use of fluorescent nucleobase analogues as labels in biotechnological applications, such as real-time PCR,[4] and in single-molecule fluorescence studies[44] which could otherwise benefit from bright and photostable intrinsic reporters.

The nucleobase analogues of the tricyclic cytosine family, tC, tC^O and tC_{nitro}, constitute rare exceptions to these general characteristics (Figure 1). UV-melting and circular dichroism measurements have shown that these analogues base-pair selectively with guanine and stabilizes the B-DNA double helix compared to natural cytosine.[45-47] The chemical structures of tC and the nitro-substituted tC_{nitro} are built upon a phenothiazine tricyclic framework, while tC^O is derived from a phenoxazine tricyclic framework. Despite their

structural similarities, though, the fluorescence properties of the tC bases in their monomeric forms and when incorporated into DNA vary somewhat.[47-50] The free nucleoside of tC has a fluorescence quantum yield of 0.13 in H_2O at room temperature but increases to an average value of 0.2 in double-stranded DNA due to a slower non-radiative deactivation, relatively independent of neighbouring bases.[48] In contrast, the fluorescence quantum yield of tC^O is 0.30 in H_2O at room temperature but decreases to an average value of 0.22 in double-stranded DNA, slightly dependent on neighbouring bases, due to a lower fluorescence rate constant.[47] The overall high fluorescence quantum yield, combined with a molar absorptivity of the lowest energy absorption band of ε_{max} = 9000 $M^{-1}cm^{-1}$, currently makes tC^O on average the brightest fluorescent nucleobase analogue inside the DNA double-helix. The fluorescence decays of tC and tC^O are single exponentials in double-stranded DNA which is a very convenient feature in particularly FRET measurements and strongly suggests that the tC bases have a relatively rigid and well-defined orientation inside the DNA helix.[47-48]

As opposed to the strong fluorescence of tC and tC^O, the nitro-substituted tC_{nitro} is virtually non-fluorescent in polar solvents at room temperature.[50] However, due to a low-lying intramolecular charge-transfer (CT) state the lowest energy electronic transition of tC_{nitro} is red-shifted compared to tC and tC^O (Figure 1) which makes it useful as a FRET acceptor with tC or tC^O serving as donor.[45, 50] As demonstrated in a recent study by our groups, the well-defined position and orientation of the tC bases inside double-stranded DNA facilitates a very high control of the orientation factor in the FRET efficiency.[45] This attractive feature has resulted in an additional desire to expand the nucleic acid toolbox with new and improved base analogue FRET-pair combinations which again requires fundamental knowledge about the photophysical properties of these probes.

Here we provide new insight into the fluorescence properties of the isolated tC bases and their ground and excited-state structures by means of density functional theory (DFT) calculations and steady-state UV-vis absorption and fluorescence spectroscopy. The excited-state decay processes of tC, tC^O and tC_{nitro} are successfully separated into temperature-dependent and temperature-independent terms and quantified using temperature-dependent fluorescence quantum yield measurements. DFT and time-dependent DFT (TDDFT) calculations are applied to gain insight into the ground- and excited-state geometries of the tC bases which we believe are directly related to their properties in confined biological environments, such as in double-stranded nucleic acid scenarios and in protein binding pockets. Translation of the calculated potential energy surfaces into the properties of the tC bases in DNA is therefore discussed.

Methodological section

Chemicals

Acetonitrile, tetrahydrofuran (THF) and dioxane were of spectrophotometric grade as purchased from Sigma-Aldrich and used without further purification. 2-methyltetrahydrofuran (MeTHF), also purchased from Sigma-Aldrich, was distilled prior use. Propylene glycol (PG) was obtained from Merck. The synthesis of the nucleosides of tC, tC^O and tC_{nitro} have previously been described[45, 47, 51](also commercially available from Glen Research).

UV-vis absorption and steady-state fluorescence

UV-vis absorption spectra were recorded on a Varian Cary 4000 spectrophotometer in 1 cm quartz cuvettes using pure solvent as baseline. Fluorescence spectra were recorded on a Spex Fluorolog 3 spectrofluorimeter (JY Horiba). The temperature-dependent fluorescence measurements were performed using an Oxford optistatDN cryostat and, at each temperature, measured after stabilization of the intensity (20 to 30 minutes). The temperature-dependent fluorescence quantum yields of the methylester[49] of tC in MeTHF and the nucleoside of tC_{nitro} in PG glass, THF and 1,4-dioxane were measured at an excitation wavelength of 370 nm using quinine sulfate in H_2SO_4 as reference (Φ_f = 0.55)[52]. The fluorescence quantum yield of the nucleoside of tC^O (tC^O-nuc) in MeTHF was measured relative to the tC^O-nuc in H_2O (Φ_f = 0.30)[47] at an excitation wavelength of 361 nm. Absorbances were kept below 0.05 to ensure linear response. Temperature-dependent quantum yields were calculated assuming temperature-independent oscillator strengths using the absorbance value determined at T = 295 K for tC and tC^O or at T = 184 K for tC_{nitro} (see spectra and discussion in supplementary information). A temperature-correction was made for both the change in refractive index and molar volume of MeTHF (supplementary information).

Temperature-dependent fluorescence.

It is often possible to separate the non-radiative decay rate constant of excited molecules into a temperature-dependent and a temperature-independent term. If the temperature-dependent non-radiative decay rate constant is assumed to follow an Arrhenius-type dependency the fluorescence quantum yield is given by[53]

$$\Phi_f = \frac{k_f}{k_f + k_0 + A \times \exp\left(-\frac{E_a}{RT}\right)} \quad (1)$$

where k_f is the fluorescence rate constant, k_0 is the temperature-independent non-radiative decay rate constant, A is the frequency factor, E_a is the activation energy of the temperature-dependent non-radiative decay process, R is the gas constant and T is the temperature. Denoting the fluorescence quantum yield as T approaches 0 K by $\Phi_{f,0}$ Equation 1 may be rewritten into

$$\ln\left(\frac{1}{\Phi_f} - \frac{1}{\Phi_{f,0}}\right) = -\frac{E_a}{R}T^{-1} + \ln\left(\frac{A}{k_f}\right) \quad (2)$$

which provides a means to evaluate E_a by measuring Φ_f as a function of T.

Quantum chemical calculations

All DFT geometry optimizations, including transition-state

This journal is © The Royal Society of Chemistry [year]

(TS) optimizations, were performed in the ground-state of the molecule using the B3LYP functional[54-56] as implemented in the Gaussian03 program package.[57] In the TS optimizations, the normal coordinate associated with the resulting (single) imaginary frequency was animated using GaussView. Electronic excitations were calculated using TDDFT[58-59] B3LYP/6-311+G(2d) as implemented in Gaussian03. Solvation effects were mimicked, where appropriate, by applying a continuum solvation shell (the CPCM model)[60-61] in the TDDFT calculations. The amount of HOMO→LUMO character of the lowest energy electronic transition of the investigated compounds was determined from the calculated CI-coefficients. Restricted Hartree-Fock (RHF) wavefunctions were used in all calculations.

The single-point molecular coordinates for the calculation of the potential energy surfaces were obtained from a combination of intrinsic reaction coordinate (IRC) calculations and geometry optimizations (both ground-state) starting from a TS optimized geometry.[62] For the IRC along the bending of tC and tC_{nitro} the TS was the planar geometry. For the IRC following the NO_2 rotation of tC_{nitro} the TS was the geometry having a NO_2 dihedral angle of 90° relative to the aromatic plane. For each of the isolated molecular geometries on these IRCs the singlet excited-state energies, E_S, were then determined from a TDDFT electronic excitation energy calculation (vertical excitations) as

$$E_{S_x} = E_{GS} + E_{exc} \quad (3)$$

where E_{GS} denotes the ground-state HF energy and E_{exc} is the excitation energy. The 2D PES of tC_{nitro} was reconstructed from 68 TDDFT single point calculations which, after symmetry considerations, yielded 272 coordinates on the calculated 2D potential energy surfaces. The coordinates on the PES of tC^O were extracted from a DFT B3LYP/6-311+G(2d) geometry optimization starting from the AM1 optimized, bent geometry and ending in the planar geometry of tC^O.

Results

Temperature-dependent fluorescence measurements

To quantify the deactivation pathways of the tC bases the fluorescence quantum yields were measured as a function of temperature and subsequently fitted to Equation 1 and 2 (Figure 2a and 2b, respectively). Quantum yield measurements of tC and tC^O were performed in liquid MeTHF (melting point T_G = 137 K) from 150 K to 300 K while the quantum yield of tC_{nitro} was monitored in PG glass (T_G = 214 K) from 145 K to 210 K to exclude effects resulting from changes in solvent viscosity expected to influence the excited-state dynamics of tC_{nitro} (*vide infra*). As the temperature is lowered the fluorescence intensity of all three fluorophores increases. The emission of tC_{nitro} in PG glass is unstructured and centred at λ_{max} = 550 nm (Figure S1). The emission of tC in MeTHF is centred at 475 nm and becomes slightly fine-structured upon lowering the temperature (Figure S2). The emission spectrum of tC^O, in turn, displays very fine-structured vibrational modes both at RT and upon lowering the temperature (Figure S3).

Since the fluorescence quantum yields of tC and tC^O only changes slightly within the temperature interval possible to monitor in MeTHF, and in particular do not reach plateaus of constant Φ_f at low temperatures, some considerations were needed in order to obtain the best parameters from the data. First, the values of $\Phi_{f,0}$ were determined which resulted in proportionality between $\ln(\Phi_f^{-1} - \Phi_{f,0}^{-1})$ and T^{-1}. The value of E_a determined from the slope of the corresponding plot was then constrained in a subsequent fit of Φ_f to Equation 1. Fitting of Φ_f of tC and tC^O were performed by additionally constraining the values of k_f to the ones measured in H_2O at room temperature.[47-48]

The parameters obtained in the temperature-dependent fluorescence measurements are provided in Table 1. At low temperatures the fluorescence quantum yields are found to approach maximum values of $\Phi_{f,0}$ = 0.71, 0.66 and 0.20 for tC, tC^O and tC_{nitro}, respectively, which directly relates to the relative ratio between k_f and k_0. The fluorescence rate constants of tC, tC^O and tC_{nitro} are $k_f = 4.1\times10^7$ s^{-1}, 8.8×10^7 s^{-1} and 5.4×10^7 s^{-1}, respectively, thus reflecting the relative magnitude of the lowest energy absorption bands[45, 47, 49] as predicted by the Strickler-Berg relation.[63] The temperature-independent non-radiative decay rate constants of the three investigated compounds are $k_0 = 1.7\times10^7$ s^{-1}, 4.5×10^7 s^{-1} and 2.1×10^8 s^{-1} for tC, tC^O and tC_{nitro}, respectively. As evidenced by the combination of excellent fits to both Equation 1 and 2 in Figure 2, the temperature-dependent non-radiative excited-state decay rate constants of all three compounds are well represented by the Arrhenius expression with activation energies of E_a = 0.074 eV, 0.12 eV and 0.20 eV for tC, tC^O and tC_{nitro}, respectively. The corresponding frequency factors are $A = 1.4\times10^9$ s^{-1}, 4.5×10^9 s^{-1} and 2.4×10^{13} s^{-1}, which results in temperature-dependent non-radiative rate constants at room temperature (T = 295 K) of $k_{nr,295\ K} = 7.6\times10^7$ s^{-1}, 3.9×10^7 s^{-1} and 1.1×10^{10} s^{-1} for tC, tC^O and tC_{nitro}, respectively.

It is important to note that the exact values of the rate constants, activation energies and frequency factors reported here only apply for the fluorophores in the solvents in which these parameters were measured, as evidenced by the varying fluorescence quantum yields of each of the three compounds in different solvents. However, the values obtained here provide a qualitative general insight of the decay processes of the tC bases. No phosphorescence was observed from neither of the investigated compounds at low temperatures in the solvents used.

Calculated electronic spectra of tC and tC^O

The electronic spectra of tC and tC^O were previously calculated for the AM1 optimized geometries using the semi-empirical ZINDO/S model,[47, 49] while TDDFT calculations were recently used to predict the electronic excitations of tC_{nitro}.[50] In order to gain more quantitative insight into the electronic states of all the tC bases (*vide infra*), the level of theory is enhanced in the calculations of tC and tC^O here, and the resulting spectra constitute in both cases significant improvements in the accuracy of the predicted excitation

energies and oscillator strengths (Figure 3). TDDFT with the B3LYP functional was chosen over more exact wave-function based methods due to the relatively large size of the investigated compounds.

Figure 3a shows the results of the TDDFT B3LYP/6-311+G(2d) (+CPCM for H_2O) calculated electronic spectrum of the B3LYP/6-31G(d,p) optimized geometry of tC. In general, the spectral shape of the calculated spectrum of tC using TDDFT agrees very well with the experimentally determined spectrum in H_2O (full-drawn line), both in terms of excitation energies and intensities. The spectra calculated on each of the two bent geometries of tC (*vide infra*) were identical as expected due to mirror symmetry (data not shown). The TDDFT calculations confirm that the lowest energy absorption band of tC is due to a single electronic transition, as fluorescence anisotropy and magnetic circular dichroism measurements previously have suggested.[49] The predicted excitation energy of the $S_0 \rightarrow S_1$ transition (3.36 eV) has an error of 0.05 eV compared to the peak of the absorption band in H_2O (3.31 eV) and the calculated oscillator strength of 0.092 is almost identical to the experimentally determined value of 0.095. The lowest transition of tC has 87% HOMO→LUMO character with the two frontier Kohn-Sham (KS) orbitals characterized by a considerable spatial overlap (Figure 3a insert). The KS orbitals optimized with and without the CPCM solvation model showed no significant differences (data not shown).

The TDDFT B3LYP/6-311+G(2d) (+CPCM for H_2O) calculated electronic spectrum of the B3LYP/6-31G(d,p) optimized geometry of tC^O is shown in Figure 3b. The overall appearance of the calculated electronic spectrum of tC^O agrees very well with the UV-vis absorption spectrum in H_2O. As for tC, the calculations confirm previous experiments[47] showing that the lowest energy absorption band of tC^O is the result of a single electronic transition. The predicted $S_0 \rightarrow S_1$ excitation energy of 3.43 eV is within 0.01 eV of the experimentally determined value in H_2O. The lowest energy electronic transition has 86% HOMO→LUMO character and these frontier KS orbitals share a relatively high degree of spatial overlap (Figure 3b insert). Again, no significant difference was observed between the KS orbitals optimized with and without the CPCM solvation model (data not shown).

Molecular geometries and potential energy surfaces

Due to the strict conditions set by the DNA double helix on the nucleobase analogues in terms of H-bonding, base-stacking and steric hindrances, the excellent nucleobase-mimicking properties of the tC bases are related to their molecular geometries. Previous geometry optimizations of tC and tC^O were performed using the semi-empirical AM1 model.[47, 49] In order to gain more accurate and quantitative information of their molecular geometries, DFT and TDDFT calculations were performed herein.

Two local energy minima on the potential energy surface (PES) of tC were identified from a B3LYP/6-31G(d,p) conformational search while only one (the global) minimum was found for tC^O. Calculations of the vibrational spectra confirmed that the optimized structures correspond to minima on the potential energy surface. As shown in Figure 4a thetwo local minima found for tC are mirror images corresponding to two geometries folded ~25° along the middle sulphur–nitrogen axis, identical to the ones found for tC_{nitro} at the same level of theory.[50] The ground-state geometry of tC obtained by AM1 calculations is also the folded conformation,[49] and this result is supported by the X-ray structure of the parent compound phenothiazine.[64-65]

While AM1 optimizations of tC^O shows two energy minima on the PES, corresponding to the folded structures similar to those optimized for tC and tC_{nitro},[47] the only minimum on the PES of tC^O identified by the B3LYP/6-31G(d,p) calculations corresponds to a planar structure of the tricyclic framework (Figure 4b). For the planar, DFT optimized structure of tC^O the IR frequency corresponding to the bending along the middle oxygen–nitrogen axis is small but real (ν_{bent} = 33 cm^{-1}). At the AM1 level, on the other hand, the IR frequency of the same vibrational mode is 34 cm^{-1} and 27i cm^{-1} for the bent and planar geometries, respectively (the planar conformation of tC^O was obtained by an AM1 TS optimization). The crystal structure of the tricyclic core of a tC^O derivative was previously shown also to be planar.[66-67]

The energy barrier between the two local energy minima on the potential energy surfaces or tC and tC_{nitro} was calculated at the DFT B3LYP/6-311G+(2d,p) level to be E_b = 0.056 eV and 0.049 eV, respectively, with no improvement obtained using a larger basis set. These values were calculated as $E_b = E_{TS} - E_{min}$, where the transition state energy, E_{TS}, was obtained from a TS optimization on the intrinsic reaction coordinate (IRC) between the two bent conformations and the equilibrium energy, E_{min}, was the energy of the geometry optimized to a minimum on the PES using the same basis set. The TS was identified as the planar geometry of the tricyclic framework, the only TS on the symmetric IRC between the two local energy minima (*vide infra*). The corresponding (single) imaginary frequency of 54i cm^{-1} was confirmed to be the bending along the central sulphur–nitrogen axis.

Since the ground-state potential energy surfaces of the three tC bases possess a low energy IRC following the bending along the middle sulphur/oxygen–nitrogen axis, as evidenced by the small IR frequencies reported above, the ground and excited-state potential energy surfaces of tC, tC^O and tC_{nitro} were calculated along this reaction coordinate. The PES of the ground and first excited-state of tC^O calculated at the B3LYP/6-311+G(2d) level is shown in Figure 5. The S_0 PES is found to be very shallow and centred around the planar equilibrium geometry, well below the average thermal energy at room temperature (dotted line) for conformations bent up to ±12°–15°. As a result of this shallow ground-state PES, the molecular framework of tC^O is expected to be very flexible in terms of bending along the oxygen–nitrogen axis. The S_1 PES is observed to be steeper along this coordinate, but with a planar equilibrium geometry as well.

As shown in Figure 6 the B3LYP/6-311+G(2d) calculated ground-state PES of tC possess two minima corresponding to the conformations bent at an angle of 25° and separated by the energy barrier E_b, where the average thermal energy at room temperature is denoted as reference (0.025 eV, dotted lines).

This journal is © The Royal Society of Chemistry [year]

Contrary the ground-state PES of tC, the first excited-state is predicted by the TDDFT B3LYP/6-311+G(2d) calculations to possess a planar equilibrium geometry with a steep increase in energy for bending above 8° to 10°.

The fast non-radiative decay pathways of nitroaromatics are often believed to involve an internal rotation of the NO_2 group.[68-74] Besides the bending coordinate of tC_{nitro}, the ground and excited-state energies of tC_{nitro} were therefore additionally investigated along the NO_2 twist coordinate (Figure 7). The singlet excited-state energies of tC_{nitro} were monitored up to the third lowest in energy, the S_3 having 87% (n,π^*)-character when occupying the S_0 equilibrium geometry. The results confirm that the S_0 geometry is stabilized at a bent conformation of the tricyclic framework and a NO_2 internal rotation of 0° while the S_1 and S_2 equilibrium geometries are planar, concordant with the ground and (π,π^*) excited-state potential energy surfaces of tC (Figure 7a). In contrast, the S_3 state is predicted to go towards an energy minimum at a NO_2 dihedral angle of ~20° around the N–C bond at which point it is of (n,π^*) and (π,π^*) mixed character (Figure 7b upper panel). The S_3 minimum energy of tC_{nitro} is additionally found to be a slightly less bent conformation of the tricyclic framework as compared to the S_0 equilibrium structure (~16° of S_3 compared to ~25° of S_0).

Figure 7b shows a cross-section of the calculated potential energy surfaces of tC_{nitro} along the NO_2 torsional coordinate, where excited-state classifications of the corresponding Franck-Condon excited-states are provided as inserts. The S_0 PES is observed to be relatively shallow along the NO_2 twist pathway, albeit not as shallow as that predicted for nitroperylene[69] and *p*-nitroaniline[71] where the ground-state population is believed to involve a wide distribution of NO_2-twist angles. The $S_0 \rightarrow S_1$ excitation energy of tC_{nitro} is predicted by the TDDFT calculations to increase for conformations along the NO_2 torsional coordinate (Figure 7b lower panel, black). A similar finding was previously used to explain the excited-state dynamics and fluorescence quantum yield dependency upon the excitation-wavelength of nitroperylene,[69] which we believe possesses similar photophysical characteristics as those of tC_{nitro}. Whether this wavelength dependency is also a property of tC_{nitro} remains to be investigated.

Solvent dipolaritydependency of the decay kinetics of tC_{nitro}

As shown in the lower panel of Figure 7b, the oscillator strength of the S_0–S_1 electronic transition of tC_{nitro} decreases drastically to zero at internal rotations of the nitro group > 45°. The decrease in transition probability is the result of a change in S_1 character, in which the LUMO orbital becomes localized on the NO_2 group as the conjugation with the aromatic plane is lost. This effect is illustrated in Figure 8a where the optimized KS LUMO of tC_{nitro} is visualized at three different NO_2 twist angles. As can be concluded, the LUMO loses its contribution from the aromatic π-system and turns into a pure antibonding nitro type orbital at angles above 45° to 60°, thus decreasing the transition overlap density between the ground-state and excited-state, and the concomitant decrease in oscillator strength of the S_0–S_1 transition (which is of 92% HOMO→LUMO character at all NO_2 twist angles).

The more localized LUMO in the twisted nitro configurations of tC_{nitro} increases the excited-state dipole moment along this IRC. As a result, the S_1 potential energy along the nitro torsional coordinate is highly dependent on solvent dipolarity. This is illustrated in Figure 8b where the S_1 energy of tC_{nitro} along the nitro twist IRC is plotted in two different solvents of varying dipolarity as calculated at the B3LYP/6-311+G(2d) level using a polarisable continuum solvation shell in the calculations. In the non-polar cyclohexane (CHx) the potential energy curve is steep and increases to an energy at the perpendicular nitro configuration of 0.37 eV above the planar nitro configuration while this energy difference is decreased to 0.26 eV in H_2O.

If the efficient non-radiative decay pathway of tC_{nitro} involves an internal rotation of the NO_2 group around the C–N bond (dashed arrow in Figure 8b), as suspected, the non-radiative deactivation process of tC_{nitro} may be expected to be driven by dipolar solvents as a result of the increase in the excited-state dipole moment along this pathway as described above. Indeed, this is supported by tC_{nitro} in less dipolar solvents such as THF and 1,4-dioxane in which tC_{nitro} is fluorescent with a quantum yield of Φ_f = 0.011 and 0.028, respectively. The emission band of tC_{nitro} in these solvents is centered around λ_{max} ~ 615 nm which is associated with a very large Stokes shift of ~7300 cm^{-1} (Figure 9, dashed lines). In contrast, the emission of tC_{nitro} in PG glass at 200 K is centered at λ_{max} = 530 nm corresponding to a Stokes shift of 4800 cm^{-1} as shown in Figure 9. In all cases, the excitation spectra confirmed that the observed emission was due to tC_{nitro} itself. No emission is observed from tC_{nitro} in either of the highly dipolar solvents H_2O, ACN, DMSO nor DMF. tC_{nitro} was also observed to be very weakly fluorescent in CH_2Cl_2 (not shown); however, the low solubility of tC_{nitro} in this solvent hindered a quantification of the fluorescence process which we estimate to be $\Phi_f < 0.01$.

The absorption spectra of tC_{nitro} in 1,4-dioxane, THF, PG, ACN and H_2O are also shown in Figure 9 (full-drawn lines). The absorption spectra have been normalized for the lowest energy absorption band to facilitate comparison. The absorption maximum of the neutral form of tC_{nitro} only shows minor differences in the investigated solvents. The position of the lowest energy absorption band is λ_{max} = 420 nm, 421 nm, 423 nm, 415 nm and 424 nm in 1,4-dioxane, THF, PG, ACN and H_2O, respectively.

Discussion

Decay kinetics and potential energy surfaces of tC and tC^O

Some general conclusions can be made about tC and tC^O. The temperature-dependent fluorescence measurements show that the total non-radiative decay rate constants of tC and tC^O are of the same magnitude at room temperature (~8×10^7 s^{-1}). The larger fluorescence quantum yield of tC^O is thus a result of a larger fluorescence rate constant, which, in turn, is due to a larger oscillator strength of the lowest energy electronic transition. However, whereas the non-radiative decay of tC is dominated by a temperature-dependent process 4 to 5 times

faster than the temperature-independent non-radiative decay process, the temperature-dependent and the temperature-independent non-radiative decay processes of tC^O are of similar magnitude (~4×10^7 s^{-1}). The fast temperature-dependent non-radiative decay process observed for tC is due to a smaller E_a of this process compared to the E_a of the same process in tC^O. The frequency factor for the temperature-dependent non-radiative decay process is 3 times larger in tC^O relative to that in tC.

The value of E_a corresponds to an energy barrier between two molecular coordinates on the PES of the excited-state of the molecule: the energy minimum, and the point of intersection with either the electronic ground-state PES (for IC) or an excited triplet state PES (for ISC), depending on the physical nature of the time-dependent deactivation process. The physical equivalences of k_0 and the temperature-dependent decay rate constant, $k_{nr}(T)$, are thus related to intersystem crossing (ISC) and IC. However, since the quantum yields of ISC are unknown, it is not possible to determine how ISC and IC relate to the fitted parameters of the tC bases. A very efficient ISC was previously reported for phenothiazine,[75] the parent compound of tC and tC_{nitro}.

The low energy barrier, E_b, between the two bent conformations of tC and tC_{nitro} reveals that these geometries frequently isomerize at room temperature. Since the reaction coordinate for the isomerization follows a vibrational mode, it is reasonable to assume a frequency factor of the order of $A_{bend} \sim 10^{10}$ s^{-1} which yields a rate of isomerization of $k_{iso} \sim 10^9$ s^{-1}, or roughly one interconversion for every 1 ns at room temperature. In addition, the calculated excited-state potential energy curve shows that the structures of tC and tC_{nitro} undergo a structural change from a bent to a planar conformation upon absorption of a photon. The isomerization between the two bent geometries is thus additionally activated by absorption of a photon. In an isotropic environment, however, the electronic state energies of the two isomers are identical. The radical cation of phenothiazine, important for the biological activity of its derivatives, has been predicted by DFT calculations to be planar as well, resulting in an increased aromatic resonance stability.[76]

It is noted, that the geometrical reorganization of tC upon absorption of a photon may explain the larger Stokes shift observed for tC compared to that of tC^O in H_2O (~7000 cm^{-1} compared to ~6000 cm^{-1}). The potential energy surfaces predicted in Figure 5 and Figure 6 for tC^O and tC, respectively, are additionally supported by the absorption and emission spectra of tC and tC^O in MeTHF and upon lowering the temperature (supplementary material). For tC no vibrational fine-structure is observed in the absorption spectrum at room temperature nor by lowering the temperature, while tC^O displays very distinct vibrational modes in the lowest energy absorption band at lower temperature.

Decay kinetics and potential energy surfaces of tC_{nitro}

The photophysical properties of tC_{nitro} are undoubtedly deeply associated with the nitro group. The non-fluorescent behaviour observed for tC_{nitro} in polar solvents at room temperature is a general property of nitrosubstituted aromatic compounds. Often, the fast non-radiative excited-state deactivation is suggested to involve low frequency vibrational modes associated with large amplitude motion of the NO_2 group (*e.g.* see nitrobenzene,[73] *p*-nitroaniline,[71-72] and nitroperylene[69]). The temperature-dependent fluorescence measurements and TDDFT calculations performed here support this model in the case of tC_{nitro}. The magnitude of the identified activation energy of the main deactivation channel of tC_{nitro} of E_a = 0.2 eV may very well correspond to the energy it costs to twist the NO_2 group in the first excited-state (Figure 7 and Figure 8). This E_a is ~0.1 eV larger than the corresponding values of the main non-radiative deactivation processes of tC and tC^O; however, in contrast to tC and tC^O this process completely quenches the fluorescence of tC_{nitro} due to the very rapid frequency associated with this process. Previous studies have shown that a magnitude of the frequency factor of the order of $A \sim 10^7$ s^{-1} to 10^8 s^{-1} is usually seen for a spin-forbidden ISC process, while a value of $A \sim 10^{11}$ s^{-1} to 10^{12} s^{-1} is indicative of a spin-allowed IC process.[53] Comparing these values to the very large value of $A = 2.4\times10^{13}$ s^{-1} determined for the non-radiative decay process of tC_{nitro} indicates that the main deactivation channel of this chromophore is an IC process. This huge frequency factor also suggests that the efficient non-radiative decay process is activated by a vibrational or rotational mode, which is reasonably argued to involve motion of the NO_2 group. Despite the fact that most nitroaromatics are found to be quenched efficiently by ISC, as discussed below, the observation of a fast $S_1 \rightarrow S_0$ IC process as the main deactivation channel was also recently reported for nitroperylene by Mohammed and Vauthey.[69]

A temperature-independent deactivation process of a different origin and with a relatively large rate constant of $k_0 = 2.1\times10^8$ s^{-1} is additionally identified in the temperature measurements of tC_{nitro} reported here. This process could be a spin forbidden ISC process which dominates the decay at lower temperatures, and possibly in non-polar solvents, due to a smaller fluorescence rate constant of $k_f = 5.4\times10^7$ s^{-1}. In many cases, especially for small aryl moities, the fast non-radiative decay of nitroaromatics has been assigned to an efficient ISC due to a low lying (n,π^*) state. Whether ISC or IC is the main deactivation pathway of nitroaromatics was early suggested by Khalil *et al.* to relate to the singlet (n,π^*) and (π,π^*) energy splitting and thus the relative size of the aromatic system.[77] Indeed, many smaller nitroaromatics are phosphorescent with ISC quantum yields often approaching unity.[73-74, 77-82] However, this may not be the case for tC_{nitro} since no phosphorescence is observed at low temperatures and the high frequency factor for the non-radiative decay of tC_{nitro} is indicative of an IC process (*vide supra*). In addition, the oscillator strength of the S_1–S_0 transition of tC_{nitro} is much stronger than what is expected for an (n,π^*) transition. The TDDFT calculations reported here predict the (n,π^*) singlet-state of tC_{nitro} to lie ~1 eV above the S_1, and associates with a considerable reorganization in this excited-state (Figure 7). CAS-SCF calculations of nitrobenzene have previously shown a distortion of the NO_2 group in the mixed (n,π^*) and (π,π^*)

This journal is © The Royal Society of Chemistry [year]

excited-state of this nitroaromatic compound.[83] A survey into the possible ISC processes of tC_{nitro}, however, is beyond the scope of this article.

In the fluorescence measurements of tC_{nitro} performed here, the very large Stokes shift of 7300 cm^{-1} observed in THF and 1,4-dioxane is strongly indicative of a CT transition, as predicted by TDDFT calculations.[50] The somewhat smaller Stokes shift observed for tC_{nitro} in PG glass compared to in liquid THF and 1,4-dioxane very likely comes as a result of the difference in solvent viscosity: For tC_{nitro} dissolved in PG glass, the solvent molecules are immobilized around the solute and solvent relaxation is therefore hindered during the excited-state lifetime, which is not the case for tC_{nitro} in THF and 1,4-dioxane at room temperature.

The predicted increase in rotational energy of the nitro group with decreasing solvent polarity can account for the increasing fluorescence quantum yield of tC_{nitro} in less dipolar solvents. Although care should be taken when evaluating the exact quantitative energy shifts calculated in different solvation shells here, the qualitative interpretation is straightforward and indeed valid in the discussion of the solvatochromic photophysics of tC_{nitro}. As a result of the structural change accompanying the decay of the intramolecular CT state of tC_{nitro}, the excited-state dynamics of tC_{nitro} may be expected to depend not only on solvent dipolarity, but also viscosity and H-bonding properties.[84-85] Of particular analogy to the case of tC_{nitro}, Hicks and coworkers argued that the E_a between planar and twisted polar states of isomers of *p*-dimethylaminobenzonitrile decreases with increasing solvent polarity.[84] The increase in excited-state dipole moment for geometries of nitroaromatics with increasing NO_2 twist angles was also predicted early by Sinha and Yates in simple theoretical models using modified Hückel theory.[86] Also, polar solvents has been reported to induce fast $S_1 \rightarrow S_0$ IC in *p*-nitroaniline,[87] and the fluorescence quantum yield of nitroperylene is observed to increase with decreasing solvent polarity.[69] However, to the best of our knowledge this has not been directly linked to an increase in excited-state dipole moment as predicted here, although we believe similar considerations as those suggested here apply to other nitroaromatics as well.

Molecular geometries of the tC bases positioned in DNA

The surrounding anisotropic nanoenvironment of the base analogues positioned in double-stranded DNA most certainly perturb their potential energy surfaces, in particular the low energy reaction coordinates associated with out-of-plane motion. The low energy IRC following the bending along the middle S–N axis of tC or tC_{nitro} and the O–N axis of tC^O will therefore be influenced by neighbouring bases both in terms of the type of nucleobase (pyrimidine or purine) and its position relative to the base analogue (5' or 3'). Although we have not performed careful calculations on the tC bases positioned in DNA, some features can be rationalized on the basis of the potential energy surfaces of the free monomers.

In the case of tC^O, the otherwise very shallow potential energy curve (Figure 5) is probably narrowed in the rigid π-stacking environment of double-stranded DNA. The observed vibrationally fine-structured emission of tC^O only in double-stranded DNA is very likely a result of this feature.[47] In the case of tC and tC_{nitro}, the small energy barrier between the two bent conformations, combined with the fact that they will isomerize upon absorption of a photon, very likely facilitates an efficient selective isomerization in double-stranded DNA to the energetically preferable isomer. This is illustrated in Figure 10 where proposed potential energy curves of tC and tC_{nitro} along the bending of the tricyclic framework are shown for the free monomeric forms (Figure 10a) and when incorporated in between two nucleobase neighbours in a B-DNA scenario (Figure 10b). The radiative processes between S_0 and S_1 are indicated as full-drawn lines while the geometrical reorganizations occurring upon absorption and emission of a photon are shown as dashed arrows. As can be seen, the IRC along the bending is suggested to be perturbed from symmetry as a result of the highly anisotropic base-stacking environment of double-stranded DNA towards the 5' and 3' directions (Figure 10c). In the example shown, the structure of tC (or tC_{nitro}) is thus energetically guided into the isomer which is directed away from the 5'-C and into the major groove. Two rough single-point AM1 energy calculations of the two bent conformations of tC positioned in between C neighbours in a B-DNA geometry (*i.e.* the two configurations shown in Figure 10c right) supported this model, showing an energy difference of as much as ~1 eV between the two conformations, primarily due to an unfavorable steric interaction with the 5'-C. This example is illustrative in that other neighbouring bases will influence the potential energy surfaces of the tC bases differently.

Generally speaking, we propose that the geometries of the tC bases positioned in confined biological environments is naturally optimized to the conformation being most favorable to the overall energy, as a result of the flexible nature of the tricyclic frameworks. This insight may be an important factor in explaining the properties of the tC bases in nucleic acid contexts and their ability to adapt to different highly anisotropic and confined environments such as those found inside various nucleic acid systems[46-48, 88] and in protein binding pockets[89-91].

Conclusions

We identified one low energy geometrical reaction coordinate on the PES of tC and tC^O and two intrinsic reaction coordinates on the PES of tC_{nitro} important for their ground and excited-state structural properties. The structure of tC^O is predicted to be very flexible in terms of bending around the central oxygen–nitrogen axis but possess a planar equilibrium geometry. The ground-state potential energy surface of tC and tC_{nitro}, both having a sulphur in the central ring, possess two energy minima corresponding to geometries bent along the middle S–N axis and separated by an energy barrier of ~0.05 eV. After excitation to the first electronically excited-state the tricyclic framework of tC and tC_{nitro} changes to a planar equilibrium geometry from which the molecule either decays directly to the S_0 by emission of radiation or by a non-radiative deactivation process. The stronger fluorescence of tC^O compared to tC is due to a larger oscillator strength of the

lowest energy electronic transition. The total non-radiative decay rate constants of tC and tC^O are of almost equal magnitude at room temperature, however, the non-radiative decay of tC is dominated by a temperature-dependent process, whereas tC^O decays non-radiatively by an almost equal combination of temperature-dependent and temperature-independent processes. The lack of fluorescence from tC_{nitro} at room temperature, on the other hand, is mainly due to an efficient temperature-dependent decay process. This is suggested to be an internal conversion process associated with rotational or vibrational modes of the NO_2 group as indicated by the very high frequency factor. If the NO_2 group twists in the excited-state along the pathway leading to IC, the excited-state dipole moment increases and may very well be the reason for the observed fluorescence from tC_{nitro}, and related nitroaromatics, in less dipolar solvents with a fluorescence quantum yield decreasing with increasing solvent dipolarity.

As a result of low energy IRCs along the bending of the tC bases they are expected to be characterized by very flexible tricyclic frameworks. In the rigid base-stacking environment provided by double-stranded DNA the otherwise very shallow S_0 potential energy curve of tC^O along the bending mode is expected to be steeper and governed by neighbouring bases. Due to the low energy barrier between the two bent conformations of tC and tC_{nitro}, combined with the fact that the excited-state equilibrium geometry is planar, we suggest that the structures of tC and tC_{nitro} positioned in DNA are naturally optimized to the conformation being most favorable to the overall energy of the DNA helix. In general, the highly flexible tricyclic frameworks of all of the tC bases predicted here help explain their properties in nucleic acid contexts as well as their ability to adapt to different kinds of confined (biological) environments such as various nucleic acid scenarios and in protein binding pockets.

Acknowledgements

This research is supported by the Swedish Research Council (VR) and the Danish Council for Independent Research | Natural Sciences (FNU).

References

1. J. N. Wilson and E. T. Kool, *Org. Biomol. Chem.*, 2006, **4**, 4265-4274.
2. M. J. Rist and J. P. Marino, *Curr. Org. Chem.*, 2002, **6**, 775-793.
3. D. W. Dodd and R. H. E. Hudson, *Mini-Rev. Org. Chem.*, 2009, **6**, 378-391.
4. U. Asseline, *Curr. Org. Chem.*, 2006, **10**, 491-518.
5. N. Venkatesan, Y. J. Seo and B. H. Kim, *Chem. Soc. Rev.*, 2008, **37**, 648-663.
6. A. Okamoto, K. Tanaka, T. Fukuta and I. Saito, *Journal of the American Chemical Society*, 2003, **125**, 9296-9297.
7. H. A. Wagenknecht, *Ann. N.Y. Acad. Sci.*, 2008, **1130**, 122-130.
8. T. Ramreddy, M. Kombrabail, G. Krishnamoorthy and B. J. Rao, *Journal of Physical Chemistry B*, 2009, **113**, 6840-6846.
9. T. Ramreddy, B. J. Rao and G. Krishnamoorthy, *Journal of Physical Chemistry B*, 2007, **111**, 5757-5766.
10. C. R. Guest, R. A. Hochstrasser, L. C. Sowers and D. P. Millar, *Biochemistry*, 1991, **30**, 3271-3279.
11. J. M. Jean and K. B. Hall, *Biochemistry*, 2004, **43**, 10277-10284.
12. M. Menger, F. Eckstein and D. Porschke, *Biochemistry*, 2000, **39**, 4500-4507.
13. O. F. A. Larsen, I. H. M. van Stokkum, B. Gobets, R. van Grondelle and H. van Amerongen, *Biophys. J.*, 2001, **81**, 1115-1126.
14. X. Shi, E. T. Mollova, G. Pljevaljcic, D. P. Millar and D. Herschlag, *Journal of the American Chemical Society*, 2009, **131**, 9571-9578.
15. C. H. Liu and C. T. Martin, *J. Mol. Biol.*, 2001, **308**, 465-475.
16. C. Hariharan and L. J. Reha-Krantz, *Biochemistry*, 2005, **44**, 15674-15684.
17. S. G. Srivatsan, N. J. Greco and Y. Tor, *Angewandte Chemie-International Edition*, 2008, **47**, 6661-6665.
18. H. Zhang, W. Cao, E. Zakharova, W. Konigsberg and E. M. De la Cruz, *Nucleic Acids Research*, 2007, **35**, 6052-6062.
19. K. Wojtuszewski, M. E. Hawkins, J. L. Cole and I. Mukerji, *Biochemistry*, 2001, **40**, 2588-2598.
20. B. W. Allan, J. M. Beechem, W. M. Lindstrom and N. O. Reich, *J. Biol. Chem.*, 1998, **273**, 2368-2373.
21. B. Holz, S. Klimasauskas, S. Serva and E. Weinhold, *Nucleic Acids Research*, 1998, **26**, 1076-1083.
22. C. Hariharan, L. B. Bloom, S. A. Helquist, E. T. Kool and L. J. Reha-Krantz, *Biochemistry*, 2006, **45**, 2836-2844.
23. R. K. Neely, G. Tamulaitis, K. Chen, M. Kubala, V. Siksnys and A. C. Jones, *Nucleic Acids Research*, 2009, **37**, 6859-6870.
24. K. D. Raney, L. C. Sowers, D. P. Millar and S. J. Benkovic, *Proc. Natl. Acad. Sci. U. S. A.*, 1994, **91**, 6644-6648.
25. C. H. Liu and C. T. Martin, *J. Biol. Chem.*, 2002, **277**, 2725-2731.
26. J. T. Stivers, K. W. Pankiewicz and K. A. Watanabe, *Biochemistry*, 1999, **38**, 952-963.
27. J. M. Jean and K. B. Hall, *Biochemistry*, 2002, **41**, 13152-13161.
28. J. M. Jean and K. B. Hall, *Proc. Natl. Acad. Sci. U. S. A.*, 2001, **98**, 37-41.
29. E. L. Rachofsky, R. Osman and J. B. A. Ross, *Biochemistry*, 2001, **40**, 946-956.
30. K. C. Thompson and N. Miyake, *Journal of Physical Chemistry B*, 2005, **109**, 6012-6019.
31. M. Mizuta, K. Seio, A. Ohkubo and M. Sekine, *Journal of Physical Chemistry B*, 2009, **113**, 9562-9569.
32. K. Miyata, R. Tamamushi, A. Ohkubo, H. Taguchi, K. Seio, T. Santa and M. Sekine, *Org. Lett.*, 2006, **8**, 1545-1548.
33. D. C. Ward, E. Reich and L. Stryer, *J. Biol. Chem.*, 1969, **244**, 1228-1237.
34. M. E. Hawkins, W. Pfleiderer, F. M. Balis, D. Porter and J. R. Knutson, *Anal. Biochem.*, 1997, **244**, 86-95.
35. T. Mitsui, M. Kimoto, R. Kawai, S. Yokoyama and I. Hirao, *Tetrahedron*, 2007, **63**, 3528-3537.
36. N. B. Gaied, N. Glasser, N. Ramalanjaona, H. Beltz, P. Wolff, R. Marquet, A. Burger and Y. Mely, *Nucleic Acids Research*, 2005, **33**, 1031-1039.
37. S. G. Srivatsan, H. Weizman and Y. Tor, *Org. Biomol. Chem.*, 2008, **6**, 1334-1338.
38. J. N. Wilson, Y. J. Cho, S. Tan, A. Cuppoletti and E. T. Kool, *ChemBioChem*, 2008, **9**, 279-285.

 This journal is © The Royal Society of Chemistry [year]

39. D. A. Berry, K. Y. Jung, D. S. Wise, A. D. Sercel, W. H. Pearson, H. Mackie, J. B. Randolph and R. L. Somers, *Tetrahedron Lett.*, 2004, **45**, 2457-2461.
40. A. Okamoto, Y. Saito and I. Saito, *J. Photochem. Photobiol. C-Photochem. Rev.*, 2005, **6**, 108-122.
41. M. E. Hawkins, *Cell Biochem. Biophys.*, 2001, **34**, 257-281.
42. S. Bharill, P. Sarkar, J. D. Ballin, I. Gryczynski, G. M. Wilson and Z. Gryczynski, *Anal. Biochem.*, 2008, **377**, 141-149.
43. J. R. Lakowicz, *Principles of Fluorescence Spectroscopy*, 3rd edn., Springer, New York, 2006.
44. F. Ritort, *J. Phys.-Condes. Matter*, 2006, **18**, R531-R583.
45. K. Börjesson, S. Preus, A. H. El-Sagheer, T. Brown, B. Albinsson and L. M. Wilhelmsson, *Journal of the American Chemical Society*, 2009, **131**, 4288-4293.
46. K. C. Engman, P. Sandin, S. Osborne, T. Brown, M. Billeter, P. Lincoln, B. Nordén, B. Albinsson and L. M. Wilhelmsson, *Nucleic Acids Research*, 2004, **32**, 5087-5095.
47. P. Sandin, K. Börjesson, H. Li, J. Mårtensson, T. Brown, L. M. Wilhelmsson and B. Albinsson, *Nucleic Acids Research*, 2008, **36**, 157-167.
48. P. Sandin, L. M. Wilhelmsson, P. Lincoln, V. E. C. Powers, T. Brown and B. Albinsson, *Nucleic Acids Research*, 2005, **33**, 5019-5025.
49. L. M. Wilhelmsson, P. Sandin, A. Holmén, B. Albinsson, P. Lincoln and B. Nordén, *Journal of Physical Chemistry B*, 2003, **107**, 9094-9101.
50. S. Preus, K. Börjesson, K. Kilså, B. Albinsson and L. M. Wilhelmsson, *J. Phys. Chem. B.*, 2010,**114**, 1050-1056.
51. P. Sandin, P. Lincoln, T. Brown and L. M. Wilhelmsson, *Nat. Protoc.*, 2007, **2**, 615-623.
52. J. N. Demas and G. A. Crosby, *J. Phys. Chem.*, 1971, **75**, 991-&.
53. J. B. Birks, *Organic Molecular Photophysics*, John Wiley and Sons, London, 1973.
54. A. D. Becke, *J. Chem. Phys.*, 1993, **98**, 5648-5652.
55. C. T. Lee, W. T. Yang and R. G. Parr, *Phys. Rev. B*, 1988, **37**, 785-789.
56. P. J. Stephens, F. J. Devlin, C. F. Chabalowski and M. J. Frisch, *J. Phys. Chem.*, 1994, **98**, 11623-11627.
57. M. J. *e. a.* Frisch, *Gaussian 03, Revision E.01*, (2004) Gaussian, Inc., Wallington Ford CT.
58. K. Burke, J. Werschnik and E. K. U. Gross, *J. Chem. Phys.*, 2005, **123**.
59. M. A. L. Marques and E. K. U. Gross, *Annu. Rev. Phys. Chem.*, 2004, **55**, 427-455.
60. V. Barone and M. Cossi, *J. Phys. Chem. A*, 1998, **102**, 1995-2001.
61. A. Klamt and G. Schuurmann, *J. Chem. Soc.-Perkin Trans. 2*, 1993, 799-805.
62. F. Jensen, *Introduction to Computational Chemistry*, 2 edn., John Wiley & Sons, 2007.
63. S. J. Strickler and R. A. Berg, *J. Chem. Phys.*, 1962, **37**, 814-&.
64. J. D. Bell, J. F. Blount, O. V. Briscoe and H. C. Freeman, *Chem. Commun.*, 1968, 1656-&.
65. J. J. H. McDowell, *Acta Crystallogr. B*, 1976, **32**, 5-10.
66. C. J. Wilds, M. A. Maier, M. Manoharan and M. Egli, *Helvetica Chimica Acta*, 2003, **86**, 966-978.
67. C. J. Wilds, M. A. Maier, V. Tereshko, M. Manoharan and M. Egli, *Angewandte Chemie-International Edition*, 2002, **41**, 115-117.
68. S. A. Kovalenko, R. Schanz, V. M. Farztdinov, H. Hennig and N. P. Ernsting, *Chem. Phys. Lett.*, 2000, **323**, 312-322.
69. O. F. Mohammed and E. Vauthey, *J. Phys. Chem. A*, 2008, **112**, 3823-3830.
70. J. A. Mondal, M. Sarkar, A. Samanta, H. N. Ghosh and D. K. Palit, *J. Phys. Chem. A*, 2007, **111**, 6122-6126.
71. V. M. Farztdinov, R. Schanz, S. A. Kovalenko and N. P. Ernsting, *J. Phys. Chem. A*, 2000, **104**, 11486-11496.
72. V. Kozich, W. Werncke, J. Dreyer, K. W. Brzezinka, M. Rini, A. Kummrow and T. Elsaesser, *J. Chem. Phys.*, 2002, **117**, 719-726.
73. M. Takezaki, N. Hirota and M. Terazima, *J. Phys. Chem. A*, 1997, **101**, 3443-3448.
74. R. Morales-Cueto, M. Esquivelzeta-Rabell, J. Saucedo-Zugazagoitia and J. Peon, *J. Phys. Chem. A*, 2007, **111**, 552-557.
75. M. Barra, G. S. Calabrese, M. T. Allen, R. W. Redmond, R. Sinta, A. A. Lamola, R. D. Small and J. C. Scaiano, *Chem. Mat.*, 1991, **3**, 610-616.
76. D. H. Pan and D. L. Phillips, *J. Phys. Chem. A*, 1999, **103**, 4737-4743.
77. O. S. Khalil, H. G. Bach and S. P. McGlynn, *J. Mol. Spectrosc.*, 1970, **35**, 455-&.
78. J. S. Zugazagoitia, C. X. Almora-Diaz and J. Peon, *J. Phys. Chem. A*, 2008, **112**, 358-365.
79. H. Ohtani, T. Kobayashi, K. Suzuki and S. Nagakura, *Bull. Chem. Soc. Jpn.*, 1980, **53**, 43-47.
80. Rusakowi.R and A. C. Testa, *Spectrochimica Acta Part a-Molecular Spectroscopy*, 1971, **A 27**, 787-&.
81. R. W. Anderson, Hochstra.Rm, H. Lutz and G. W. Scott, *Chem. Phys. Lett.*, 1974, **28**, 153-157.
82. R. Hurley and A. C. Testa, *Journal of the American Chemical Society*, 1968, **90**, 1949-&.
83. M. Takezaki, N. Hirota, M. Terazima, H. Sato, T. Nakajima and S. Kato, *J. Phys. Chem. A*, 1997, **101**, 5190-5195.
84. J. M. Hicks, M. T. Vandersall, E. V. Sitzmann and K. B. Eisenthal, *Chem. Phys. Lett.*, 1987, **135**, 413-420.
85. Z. R. Grabowski, K. Rotkiewicz and W. Rettig, *Chem. Rev.*, 2003, **103**, 3899-4031.
86. H. K. Sinha and K. Yates, *J. Chem. Phys.*, 1990, **93**, 7085-7093.
87. C. L. Thomsen, J. Thogersen and S. R. Keiding, *J. Phys. Chem. A*, 1998, **102**, 1062-1067.
88. L. M. Wilhelmsson, A. Holmén, P. Lincoln, P. E. Nielson and B. Nordén, *Journal of the American Chemical Society*, 2001, **123**, 2434-2435.
89. P. Sandin, G. Stengel, T. Ljungdahl, K. Borjesson, B. Macao and L. M. Wilhelmsson, *Nucleic Acids Research*, 2009, **37**, 3924-3933.
90. G. Stengel, J. P. Gill, P. Sandin, L. M. Wilhelmsson, B. Albinsson, B. Nordén and D. Millar, *Biochemistry*, 2007, **46**, 12289-12297.
91. G. Stengel, B. W. Purse, L. M. Wilhelmsson, M. Urban and R. D. Kuchta, *Biochemistry*, 2009, **48**, 7547-7555.

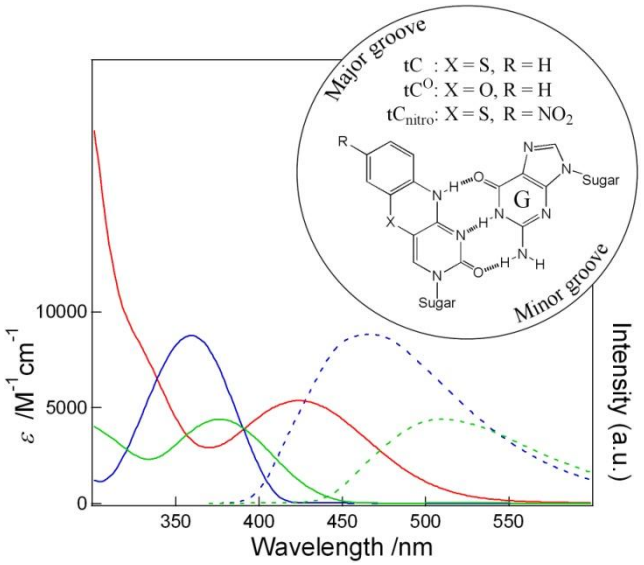

Figure 1. UV-vis absorption (full-drawn) and fluorescence spectra (dashed) of the monomeric forms of tC (green), tC^O (blue) and tC$_{nitro}$ (red) in H_2O. Insert: chemical structures of the tricyclic cytosine analogues in their base-pairing environment with guanine. Also shown is the direction of major and minor groove when looking down the long axis of double-stranded DNA.

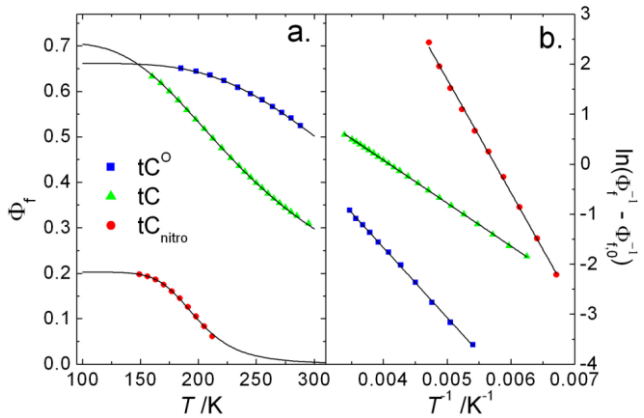

Figure 2. Temperature dependence of the fluorescence quantum yield of tC, tC^O and tC$_{nitro}$. Measurements were performed in MeTHF for tC and tC^O, and in PG glass for tC$_{nitro}$. **a)** Solid lines are plots of Equation 1 with the parameters shown in Table 1. **b)** Solid lines are plots of the experimental data using Equation 2 with the parameters given in Table 1. Absorption and emission spectra are provided in supplementary material.

Table 1. First excited-state decay parameters of tC and tC^O in MeTHF and tC$_{nitro}$ in PG glass.

	k_f /s^{-1}	k_0 /s^{-1}	$k_{nr,295\,K}$ [a] /s^{-1}	A /s^{-1}	E_a /eV	Φ_f [b]
tC	4.1×10^7	1.7×10^7	7.6×10^7	1.4×10^9	0.074	0.3
tC^O	8.8×10^7	4.5×10^7	3.9×10^7	4.5×10^9	0.12	0.5
tC$_{nitro}$	5.4×10^7	2.1×10^8	1.1×10^{10}	2.4×10^{13}	0.20	0.0

[a] Temperature-dependent non-radiative decay rate constant at T = 295 K calculated as $k_{nr} = A \times \exp[-E_a/(RT)]$.

[b] Fluorescence quantum yield at T = 295 K.

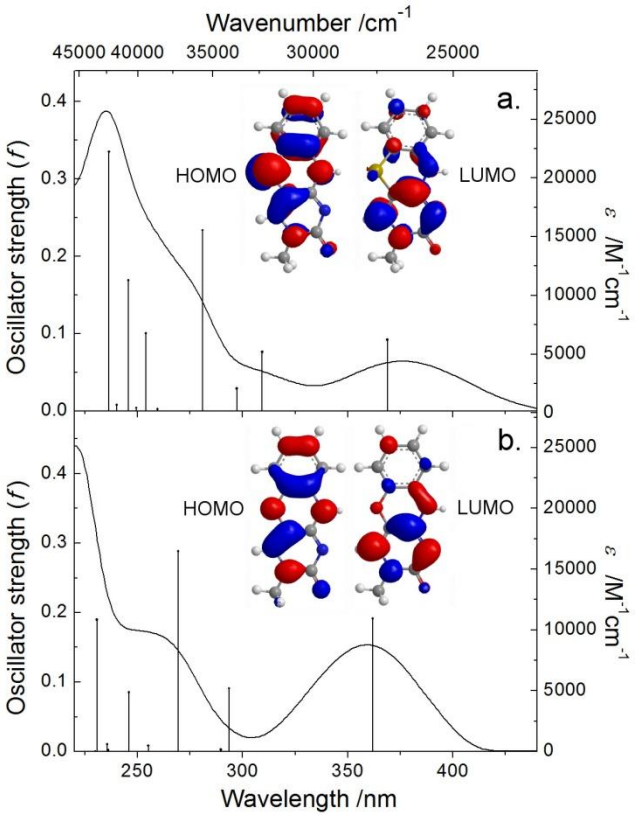

Figure 3. Ten lowest energy electronic transitions of **a)** tC, and **b)** tC^O compared to the experimental UV-vis absorption spectra in H_2O (full-drawn). Frontier KS orbitals are shown as inserts. Calculations were performed on the B3LYP/6-31G(d,p) optimized geometries using TDDFT B3LYP/6-311+G(2d) with a CPCM solvation model for H_2O.

This journal is © The Royal Society of Chemistry [year]

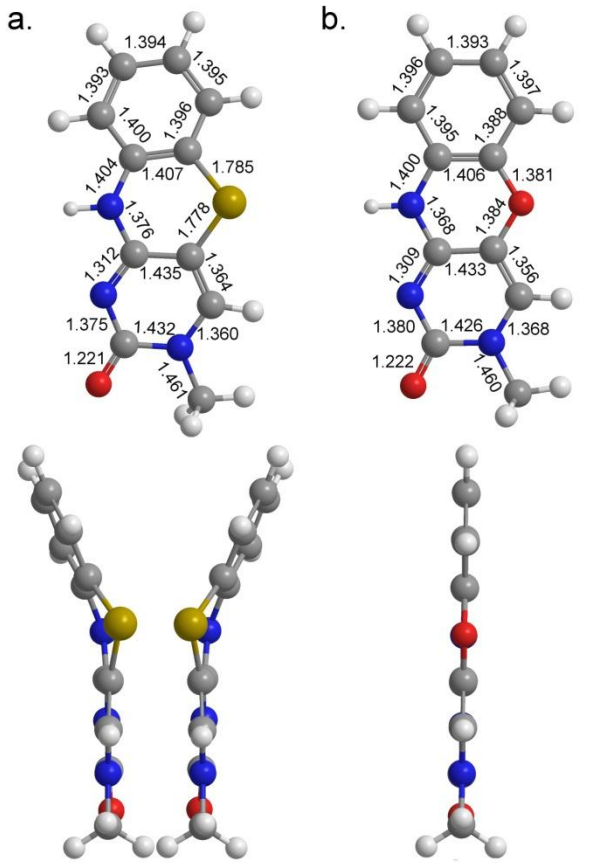

Figure 4. B3LYP/6-31G(d,p) optimized ground-state structures of **a)** tC, and **b)** tC^{O}. Top: Frontview. Bottom: Sideview (both local energy minima of tC are shown). Elements are labeled as follows: H white; C grey; N blue; O red; S yellow. Bond lengths are given in Ångströms.

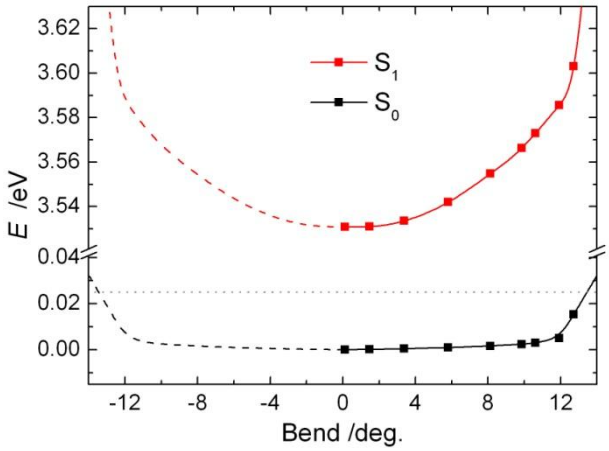

Figure 5. PES of tC^{O} following the coordinate for bending along the middle oxygen-nitrogen axis as calculated at the TDDFT B3LYP/6-311+G(2d) level. Full-drawn lines are guides for the eye, and dashed lines are mirror-images of the calculated points. The dotted grey reference line denotes the thermal energy at T = 295 K.

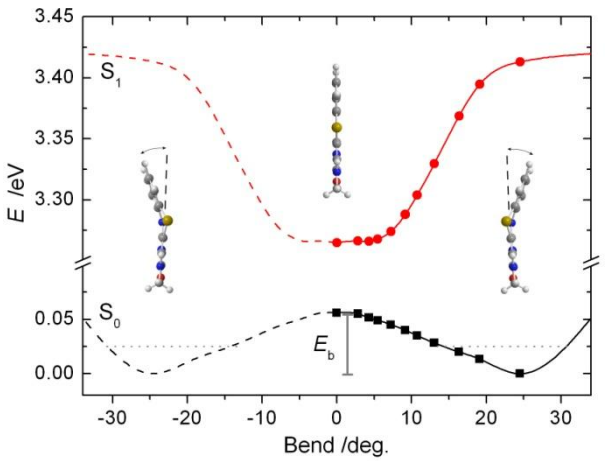

Figure 6. S_0 and S_1 potential energy surfaces of tC following the coordinate of bending along the middle sulphur-nitrogen axis. Full-drawn lines are guides for the eye, and dashed lines are mirror-images of the calculated points. E_b = 0.05 eV denotes the ground-state energy barrier between the two bent geometries. The dotted grey reference line denotes the thermal energy at T = 295 K. Calculations were performed at the B3LYP/6-311+G(2d) level.

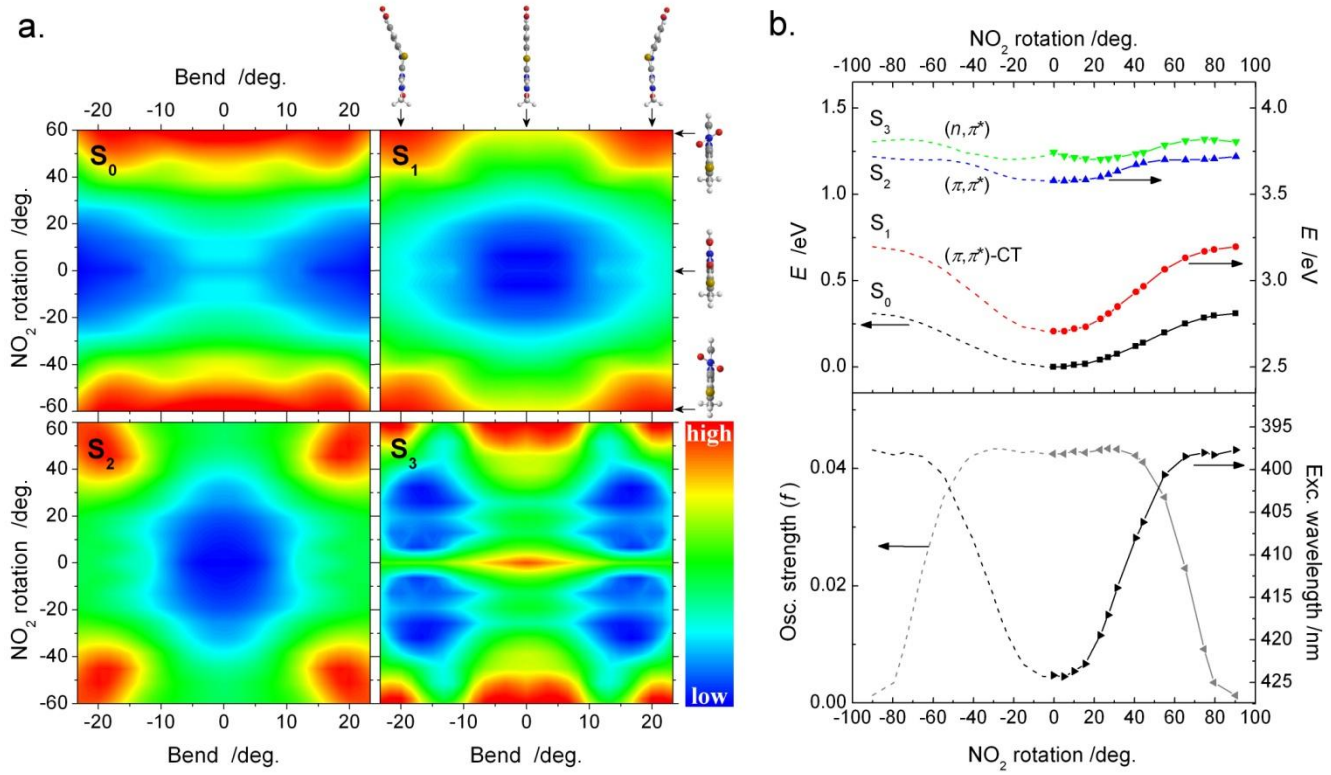

Figure 7. Potential energy surfaces of the ground and the three lowest electronically excited singlet states of tC_{nitro}. **a)** 2D PES following the coordinates of bending along the middle sulphur-nitrogen axis (horizontal axis) and NO_2 rotation (vertical axis). The shown color scale increases linearly from blue→red (low→high) as follows: S_0 0.00→0.25 eV; S_1 2.53→3.10 eV; S_2 3.48→3.72 eV; S_3 3.67→3.80 eV. **b)** Cross section following the NO_2 rotation coordinate at bent = 25°. **Upper panel:** Calculated potential energy surfaces of S_0, S_1, S_2 and S_3. Excited-state classifications are provided. **Lower panel:** $S_0 \rightarrow S_1$ Oscillator strength (grey) and excitation energy (black) dependency upon the rotation of the NO_2 group. The full-drawn lines are guides for the eyes and the dashed lines are mirror-images of the calculated points. Calculations were performed at the TDDFT B3LYP/6-311+G(2d) level.

This journal is © The Royal Society of Chemistry [year]

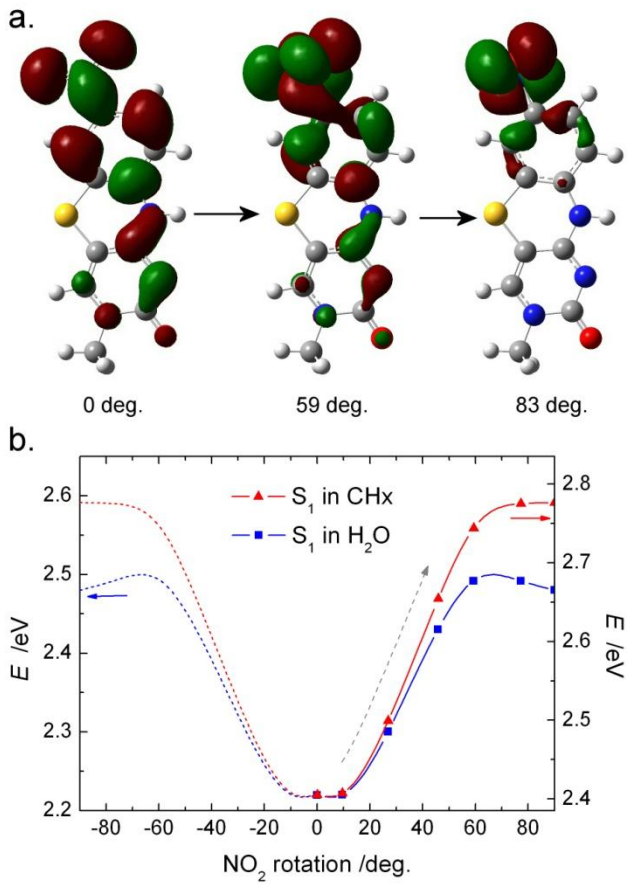

Figure 8. a) Visual representation of the LUMO of tC_{nitro} at three different degrees of NO_2 twist. **b)** Solvent polarity dependency of the S_1 state energy of tC_{nitro} following the NO_2 rotation coordinate for the flat conformation (*i.e.* bent = 0° for all calculated points). Dashed arrow denotes the proposed pathway of the main radiationless deactivation process of tC_{nitro}. Calculations were performed using TDDFT B3LYP/6-311+G(2d). Solvation effects were simulated using the CPCM model.

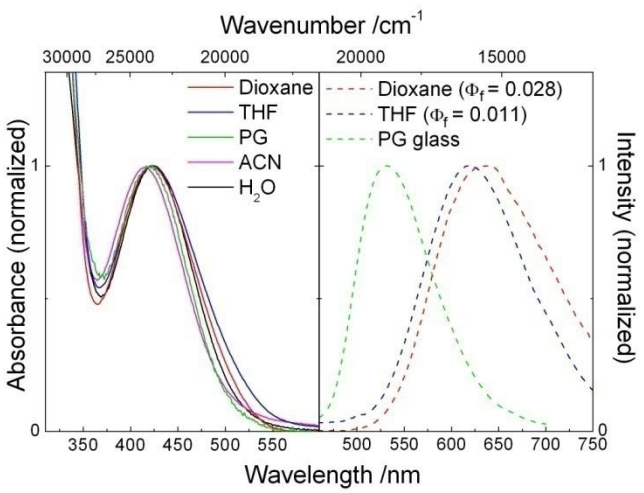

Figure 9. Absorption and emission spectra of tC_{nitro} in various solvents. Left: Isotropic absorption spectra. Right: the emission spectra of tC_{nitro} in propylene glycol glass at 200 K, and in THF and 1,4-dioxane at RT. All spectra have been normalized to facilitate comparison. Emission spectra were acquired using an excitation wavelength of 420 nm.

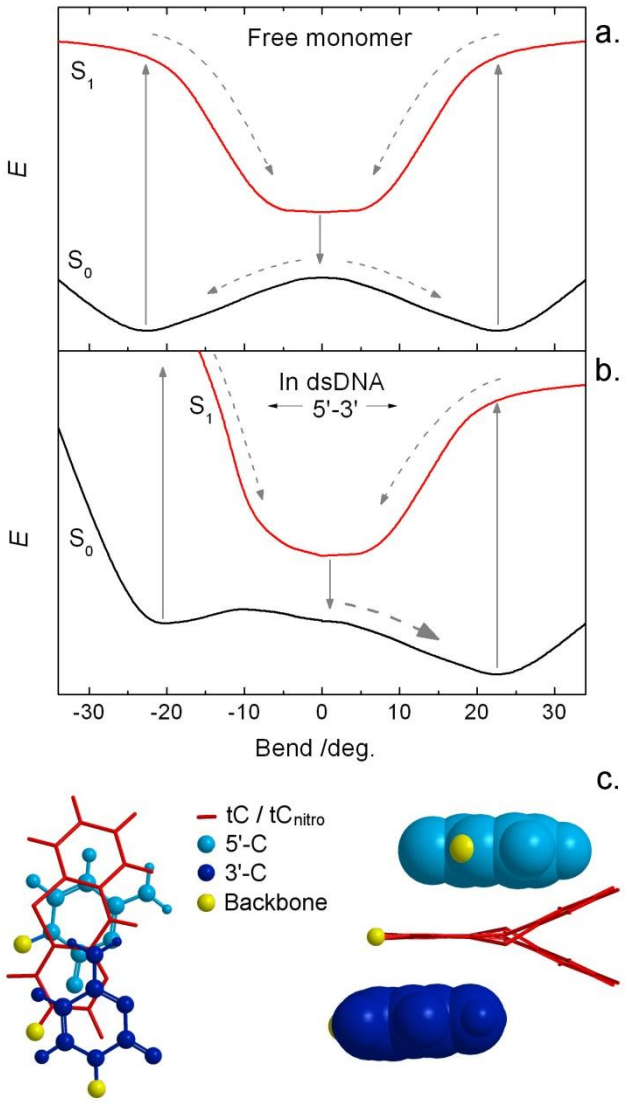

Figure 10. Hypothetical potential energy curves of ground and first excited-state of tC and tC_{nitro} following the bending along the middle sulphur-nitrogen axis in their **a)** free monomeric forms, and **b)** rigidly positioned in double-stranded DNA in between two representative C neighbours. Dashed and full-drawn arrows denote non-radiative and radiative processes, respectively. **c)** Left: base-stacking of tC/tC_{nitro} when looking down the long axis of double-stranded DNA. A 3'-C is shown on top of tC/tC_{nitro} and a 5'-C is shown below tC/tC_{nitro}. Right: same molecular coordinates as left image but projected from a sideview. In the right figure the two bent conformations of tC/tC_{nitro} are overlaid.

Graphical contents entry:

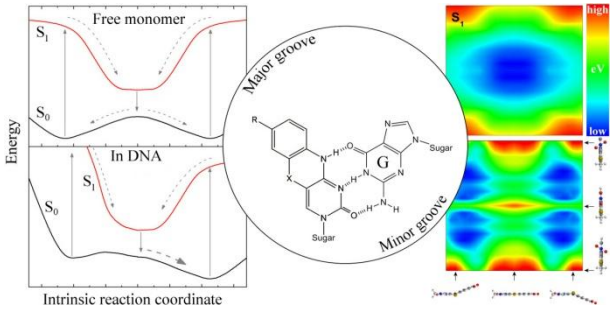

We provide new insight into the fluorescence properties and the ground- and excited-state structures of the isolated tC nucleobases important for understanding their properties in nucleic acid environments.

This journal is © The Royal Society of Chemistry [year]